Green Removal of Toxic Th(IV) by Amino-Functionalized Mesoporous TiO_2-SiO_2 Nanocomposite

Janitabar Darzi, Simin*[+]

Materials and Nuclear Fuel Research School, Nuclear Science and Technology Research Institute, P.O. Box 14395-836 Tehran, I.R. IRAN

Abdolmohammadi, Shahrzad; Latifi, Mohammad Hoseyn

Department of Chemistry, East Tehran Branch, Islamic Azad University, P.O. Box 18735-138 Tehran, I.R. IRAN

ABSTRACT: *Mesoporous TiO_2-SiO_2 nanocomposite (TS) was synthesized via sol-gel method and Amino-functionalized using 3-(aminopropyl) triethoxysilane. prepared amino-functionalized TiO_2-SiO_2 (NH_2TS) was evaluated for eliminating radioactive Th(IV) ion in comparison with (TS). The prepared nanocomposites were characterized using FT-IR, XRD, DSC-TGA, SEM, EDS, BET, and BJH analyses. DSC and TGA analyses revealed that the total organic content of the NH_2TS was at about 4%. According to the XRD patterns, synthesized nanocomposites exhibited only the crystalline anatase phase, and the sizes of the anatase crystallites in the prepared TS and NH_2TS calculated to be 10.4 and 14.1nm, respectively. Moreover, the pore diameters of TS and NH_2TS estimated to be 4.65 and 3.632 nm according to their BJH plot. The kinetic data of Th(IV) uptake process on both of two nanocomposites corresponded well to the pseudo-second-order equation. Adsorption thermodynamic parameters including the standard enthalpy, entropy, and Gibbs free energy revealed that the ion exchange reactions on both of NH_2TS and TS nanocomposites were endothermic and spontaneous processes. The results indicated that NH_2TS exhibited higher adsorption affinity toward Th(IV) compared to TS. Moreover, based on the Langmuir model, the maximum adsorption capacity of NH_2TS nanocomposite towards the Th (IV) was found to be 1000 mg/g.*

KEYWORDS: *TiO_2-SiO_2; Amino-functionalization; Th (IV) ion removal; Nanocomposite; Gibbs free energy.*

INTRODUCTION

Thorium has received great attention owing to its unique properties and a wide range of applications. Thorium, as an alternative to uranium, has found multiple applications as a nuclear fuel in power plants. Unlike uranium, thorium and its compounds pave the way for widespread industrial productions common as well as high-temperature ceramics, carbon arc lamps, strong alloys, and catalysts [1]. Radioactive thorium intake albeit in small quantities with water, or at the working place under the shadow of this element. Unfortunately, thorium remains in the body, emitting harmful alpha radiation as it decays. The danger of developing leukemia, liver

* *To whom correspondence should be addressed.*
+ *E-mail: sjanitabar@aeoi.org*
1021-9986/2020/2/191-202 12/$/6.02

and bile duct cancer in the industrial workers dealing with thorium has been estimated to be well above 20 times the risk of the rest of the population [2]. So, adverse effects of thorium contamination necessitate its clean up, a great challenge to human society. A good number of processes for the scooping of thorium ions out of wastewaters and radioactive wastes by natural and synthetic materials have been reported [3]. Adsorption technology has been confirmed to be an effective method for heavy metals enrichment and clean up by using a series of adsorbent materials, such as carbon nanotubes, activated carbons [4], zeolite, porous alumina, etc [5–7]. However, the reported low adsorption capacity is unsatisfactory and undesirable for universal application of the unclear technology. Hence, new sorbents with high adsorption capacities for eliminating harmful radionuclides are required [8]. Some of the surface functionalized nano oxides are known as promising materials with improved adsorption capacity [9-11]. In this research, titania-silica mixed oxide as a recognized sorbent in the field of eliminating hazardous heavy metal ions with cation exchange property of SiO_2 and both cation and anion exchange properties of TiO_2 [12] was applied for amino functionalization and adsorption studies towards thorium (IV) ion removal. Sorption of Th(IV) on amino functionalized and non-functionalized TiO_2-SiO_2 were evaluated versus time, pH, and temperature. The thermodynamic data such as ΔH^0, ΔS^0 and ΔG^0 were calculated from temperature relevant sorption isotherms and used to investigate the sorption properties of Th(IV) on amino-functionalized TiO_2-SiO_2 nanocomposite.

EXPERIMENTAL SECTION

Materials

Titanium tetrachloride ($TiCl_4$, 99.9%) was purchased from Fluka. Tetraethylorthosilicate (TEOS, 98%), HNO_3 (70 wt%, d=1.42gcm^{-1}), NH_4OH (25 wt%), APTES (3-aminopropyltriethoxysilane), anhydrous ethanol (C_2H_5OH) and thorium nitrate pantahydrate ($Th(NO_3)_4.5H_2O$) were supplied by Merck.

TS and NH_2TS Preparation

TiO_2-SiO_2 nanocomposite (TS) was provided using the method previously described [13]. The reaction sequence for the synthesis of TS is summarized as follows:

$TiCl_4$ was added to water under stirring in an ice water bath. The prepared dispersion was treated with NH_4OH and the pH was adjusted to 7. The produced solid was collected via filtration and washed with water. The resulted precipitate was dispersed in 200mL of 0.3 mol/L HNO_3. The mixture was refluxed under stirring at 70°C for 16 h. After that, 25mL of tetraethylorthosilicate was added dropwise to the above prepared sol and stirred at 70°C. The produced powder was filtered and washed with water and then dried at room temperature. The prepared mixed oxide was calcined in air, at 400°C for 1 h. The prepared powder was labeled as TS.

In order to prepare amino- functionalized TiO_2-SiO_2, 1.2 g of the synthesized TS powders was dispersed in 200 mL ethanol. After that, 2mL of 3-aminopropyltriethoxysilane (APTES) was added to the suspension and the mixture was refluxed for 7 h. The powders were filtered and washed with ethanol and water several times. The powder dried at room temperature was labeled as NH_2TS.

Characterization of prepared adsorbents

X-ray powder diffractometry was carried out using an 1800 PW Philips diffractometer with CuKa beam and the average crystallite size of the synthesized samples was determined by Scherrer equation [14]. The infrared spectra were recorded using a Brucker-Vector22 spectrometer. The morphology of the products was studied by Scanning Electron Microscopy (SEM, Philips XL30). Oxford INCA Energy-Dispersive X-ray (EDX) was used to analyze the elemental constituents of amino-functionalized composite. The Brunauer–Emmett–Teller (BET) specific surface area and Barret–Joyner–Halenda (BJH) pore size distribution plot of the samples were determined through nitrogen adsorption–desorption (Quantachrome NOVA 2200 e). ThermoGravimetry and Differential Scanning Calorimetry (TG–DSC) was carried out using STA 150 Rhenometric Scientific unit. Measurements were taken at a heating rate of 10 °C/min from 25 to 800°C in argon atmosphere.

Adsorption experiments

Batch experiments using TS and NH_2TS composite adsorbents and 200 mg/L initial thorium ion concentration were conducted to investigate the effects of solution pH, temperature and contact time on sorption performance of the prepared composites.

Th(IV) solutions were placed in 50 mL polypropylene bottles and 0.1 g of sorbent was added to each of the test solution. After that, the sample bottles were placed in a thermostated shaker. After regular time intervals, the suspensions were centrifuged and then the supernatant solutions were passed through milipore filters to remove the suspended sorbents particles. Finally, the concentration of Th(IV) was determined by Inductively Coupled Plasma-Atomic Emission Spectroscopy (ICP–AES). The experiments were adjusted at 298.15 K and pH 5 except for the temperature and pH dependence studies. NaOH and HNO_3 solutions were used to adjust the pH values, monitored with a digital pH meter.

The amount of adsorbed thorium ion was presented in terms of the distribution coefficient (Kd). The distribution coefficient (Kd) of adsorbed Th(IV) on the composite adsorbents was calculated according to the following equation:

$$K_d = \frac{C_0 - C_e}{C_e} \times \frac{V}{m}(mL/g) \quad (1)$$

where C_0 and C_e are the initial and final Th(IV) ion concentrations in the aliquots, respectively. V (mL) is the solution volume and m (g) is the mass of sorbent. A higher Kd reveals a higher selectivity or adsorption.

The adsorption Th (IV) ions expressed in terms of adsorption percentage (Ads %) was obtained from Eq. (2)

$$Ads\% = \frac{C_0 - C_e}{C_0} \times 100 \quad (2)$$

The effect of temperature on Th (IV) adsorption was examined between 288.15 K and 308.15 K. Furthermore, the thermodynamic parameters such as ΔH^0, ΔS^0 and ΔG^0 were calculated.

RESULTS AND DISCUSSION

Characterization of TS and NH_2TS

Differential scanning calorimetry and thermo-gravimetric curves of synthesized NH_2TS are shown in Fig. 1. The decrease in weight, up to 100°C is related to desorption of the physically sorbed water which is confirmed by a small endothermic peak on the DSC curve. The total organic content of the mater determined from the total mass weight, apart from water loss stage, is 4%. Thermal organic weight loss follows a two step process, the first one illustrates an explicit exothermic peak on the DSC curve at 300°C attributed to the presence of amine groups [15, 16].The second one correspond to the decomposition of organic moieties from the organosilane [15, 17].

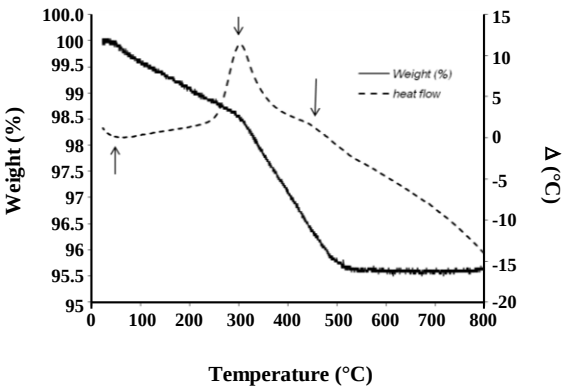

Fig. 1: TG-DSC curves of TiO_2-SiO_2 functionalized with APTES.

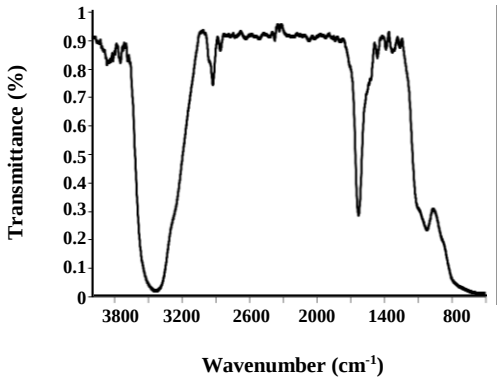

Fig. 2: FT-IR spectra of TiO_2-SiO_2 functionalized with APTES.

IR spectra of NH_2TS samples are shown in Fig. 2. The band at around 1100 cm^{-1} is the asymmetrical vibration of the Si-O-Si bond in the tetrahedral SiO_4 unit of the SiO_2 matrix. The symmetrical Si-O-Si stretching vibration appeares at 795cm^{-1}, along with a peak at 954cm^{-1}. This band is ascribed to the vibration involving a SiO_4 tetrahedron bonded to a titanium atom through Si-O-Ti bonds. The TiO_2-SiO_2 sample shows a band at around 490cm^{-1} which is representative of the titania matrixes [13]. The broad band in the region of 3200–3650 cm^{-1} is due to the stretching vibration of hydroxyl groups and the peak at 1620 cm^{-1} can be assigned to the deformation vibration of the free water molecules [18, 19]. However,

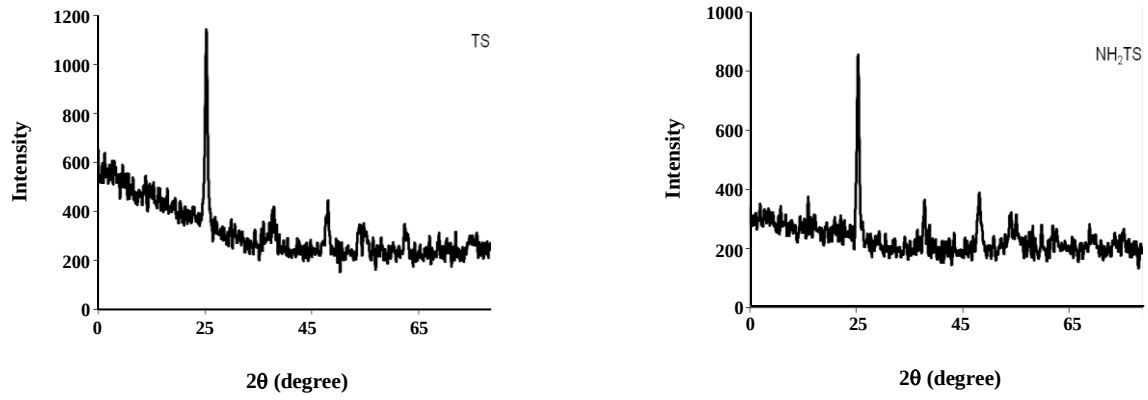

Fig. 3: XRD patterns of TS and NH_2TS samples.

according to Mureseanu et al. reports, the absorption band at 1630 cm^{-1} is not only related to the H_2O but also to the NH_2 which seems to be some indication of the presence of the amine groups [20]. The typical C–H stretching vibrations of the propyl chains at 2900 cm^{-1}, the C–H deformation vibration at 1485 cm^{-1}, and the N–H deformation vibration at 1556 cm^{-1} confirmed the grafting of amino propyl groups in the sample [21]. Two absorption bands located in the region of 3300–3500 cm^{-1} related to the symmetry and asymmetry stretching modes of NH could not be exhibited due to the overlap of the wide band of water.

The X-Ray Diffraction (XRD) analyses of TS and NH_2TS nanocomposites are shown in Fig. 3. The XRD pattern of the TS composite shows that TiO_2-SiO_2 mater has crystalline anatase phase in amorphous silica matrix. Comparing the XRD patterns of TS and NH_2TS reveals that both of the samples exhibit only anatase phase of TiO_2 and functionalization with APTES does not change the crystal structure of the mater. The sizes of the anatase crystallites in the prepared TS and NH_2TS nanocomposites measured by peak half-width according to the Scherrer equation, are calculated to be 10.4 and 14.1nm, respectively. It can be seen that the crystallite size of the obtained TS powder increases with grafting of amino groups to the mater.

Fig. 4a and b show scanning electron microscopy (SEM) images of TS and NH_2TS samples. SEM images reveal nanoscale dimensions for TS and NH_2TS particles. These images demonstrate that the morphology of the samples are not different from each other. However, the modification of TS with APTES agent enlarges the NH_2TS particles.

Fig. 4c illustrates the Energy-Dispersive X-ray spectroscopy (EDX) analysis of NH_2TS sample. On the basis of EDX analysis, the peak due to nitrogen is distinct at 0.3 KeV. Moreover, the content of nitrogen in the sample is estimated to be 3wt%.

N_2 adsorption–desorption isotherms and the pore size distribution analyses of TS and NH_2TS samples are illustrated in Fig. 5. Isotherms of TS and NH_2TS composites are of type IV which indicating the presence of mesopore. However in the case of TS the hysteresis loop is of a H_2 type with a triangular shape and a steep desorption branch. Such behavior is observed for many porous inorganic oxides and ascribed to the pore connectivity effects [22]. Indeed, H_2 hysteresis loops are observed for materials with relatively uniform channel-like pores, when the desorption branch is located under relative pressures in the proximity of a lower pressure limit of adsorption–desorption hysteresis [23].

For the amino-functionalized nanocomposite, NH_2TS, hysteresis loop is an H_4 type. Type H_4 loops feature parallel and almost horizontal branches and their occurrence has been attributed to the adsorption–desorption in narrow slit-like pores [24]. The surface area of TS and NH_2TS composite samples calculated from BET are 405.3 and 205.1m^2/g, respectively. Furthermore, the pore diameters of TS and NH_2TS are 4.65 and 3.632 nm according to their BJH plot. It can be seen that grafting the organic functional moieties on TiO_2-SiO_2 composite results in a decrease in the specific surface

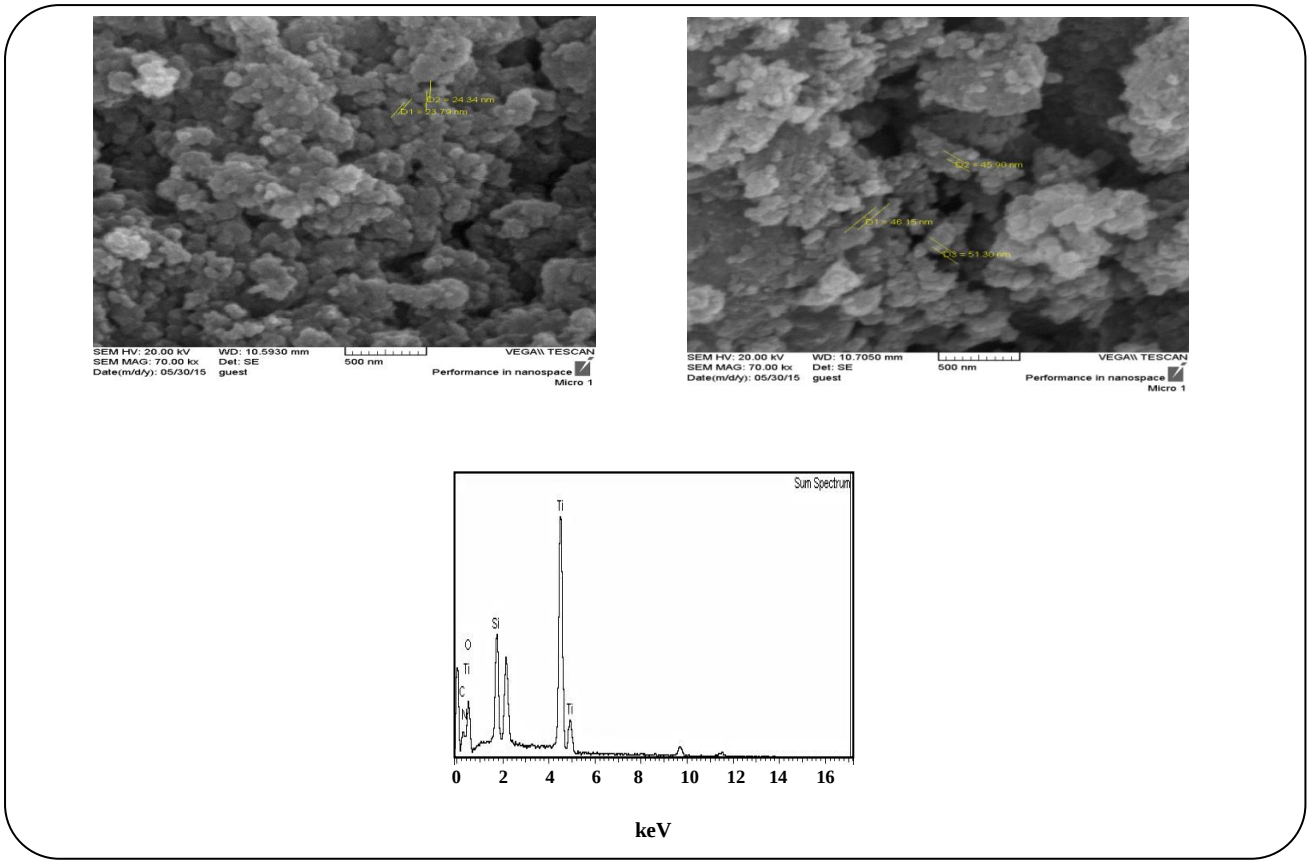

Fig. 3: XRD patterns of TS and NH_2TS samples.

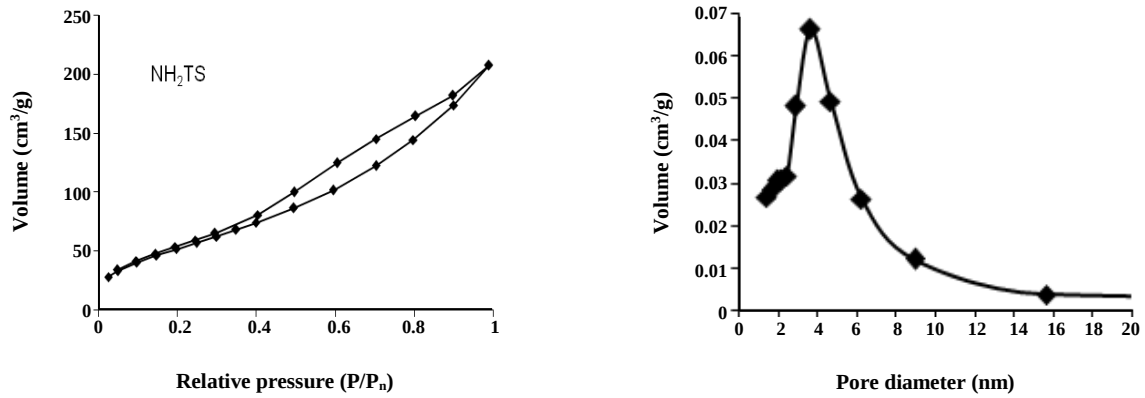

Fig. 5: N_2-adsorption–desorption isotherms and BJH pore size distribution curves of TS and NH_2TS.

area and pore size. The surface area decreases by 49% after the grafting of APTES on TS mater.

Adsorption studies

Effect of pH on thorium ion adsorption

The pH of Th(IV) solution is a controlling factor in ions sorption. The pH of the solution may affect the surface charge of the sorbent as well as the degree of ionization of the metal ions present in the solution [25]. Depending on the pH, metal ions may form complexes with OH^- such as $M(OH)_n$, $M(OH)^-_{n+1}$ and $M(OH)^{2-}_{n+2}$.[26]. Fig. 6 represents the effect of the initial pH of the solution on the adsorption percentage (Ads %) values of the Th(IV) ion on TS and NH_2TS. Results emphasize

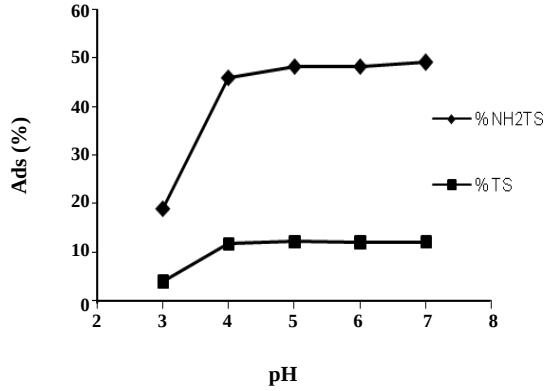

Fig. 6: Effect of pH on removal of Th (IV) onto TS and NH_2TS sorbents. Conditions: adsorbent dose 2 g/L; equilibrium time 5 h; temperature 298.15 K.

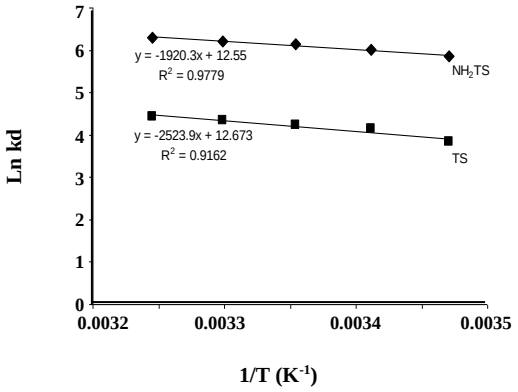

Fig. 7: The effect of solution temperature on the distribution coefficient of thorium ions on TS and NH_2TS nanocomposites.

that with enhancement of pH, the Th(IV) sorption increases in both of two systems. The increase of pH enhances the metal ion removal as a result of lowering the positive charge of the adsorbents, resulting in an increase in their attraction towards the metal cations [27]. The decrease in thorium ions sorption within low pH range could be ascribed to the competition between the excess of H^+ ions in the medium and positively charged cationic species present in the solution [28]. lower pH hinders hydrolysis of the metal ions. Moreover, the surfaces of exchangers are largely protonated at low pH. Hence, the electrical repulsion between the metal cations and positively charged surface of the sorbents brings about causing less sorption of Th(IV) ions [29–31]. *Anirudhan et al.* reported that the high adsorption at pH 5 could be ascribed to the predominance of polymerized thorium species such as $[Th_2(OH)_2]^{6+}$ possessing a better binding affinity to the sorbents [32].

Effect of temperature on removal of thorium ion and adsorption thermodynamic

The thermodynamic parameters, the values of standard free energy (ΔGº), standard enthalpy (ΔHº), and standard entropy (ΔSº) of the sorption are useful in defining whether the sorption reaction is endothermic or exothermic, and the spontaneity of the adsorption process. The amounts of ΔHº, and ΔSº were calculated from the slope and intercept of the straight line obtained from plotting ln Kd values versus reciprocal temperature (Fig. 7), respectively, by using the following equation [33]:

$$\ln K_d = \Delta S^o/R - \Delta H^o/RT \quad (3)$$

After obtaining ΔHº and ΔSº values of the adsorption, ΔGº of the adsorption process at each temperature was calculated from the well-known equation [34]:

$$\Delta G^o = \Delta H^o - T\,\Delta S^o \quad (4)$$

Thanks to Table 1, the obtained negative amounts of ΔGº at different temperatures and the positive amount of ΔHº reveal that the ion exchanger process is an endothermic and spontaneous sorption reaction on the surface of both TS and NH_2TS nanocomposites. The positive value of ΔSº and thus a decrease in the amount of ΔGº with an increase in the temperature indicate that Thorium adsorption on the sorbent is more spontaneous at higher temperatures.

The decrease of ΔG^0 with the increasing temperature indicates more efficient adsorption at higher temperatures. According to Wu and co-workers, at higher temperature, Th(IV) is readily dehydrated, and therefore, adsorption becomes more favorable [35]. The values of ΔG^0 for TS and NH_2TS at 298.15 K are -10.4152 and -15.137 kJ/mol, which indicate that the adsorption of Th(IV) on NH_2TS is more favorable than TS.

Sorption kinetics is one of the most important aspects of the adsorption process. Kinetic models control the mechanism of the adsorption process [37]. The rate of sorption of Th(IV) ions by TS and NH_2TS nanocomposites was studied by equilibrating the 0.1 g solid phase with 50 mL ion solution for different time

Table 1: Thermodynamic parameters of thorium adsorption on TS and NH_2TS nanocomposites.

NH_2TS Sorbent		TS Sorbent	
ΔH^0(kJ/mol) 15.96 ΔS^0(kJ/mol/K) 0.1043		ΔH^0(kJ/mol) 20.98 ΔS^0(kJ/mol/K) 0.1053	
Temperature (K)	ΔG^0(KJ/mol)	Temperature (K)	ΔG^0(KJ/mol)
288.15	-14.094	288.15	-9.3622
293.15	-14.6155	293.15	-9.8887
298.15	-15.137	298.15	-10.4152
303.15	-15.6585	303.15	-10.9417
308.15	-16.18	308.15	-11.4682

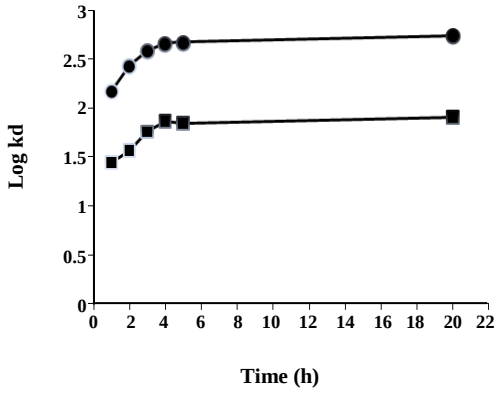

Fig. 8: Effect of the contact time on Kd of the Th(IV) ions. Experimental conditions: temperature 298.15 K, and pH of the solution 5.

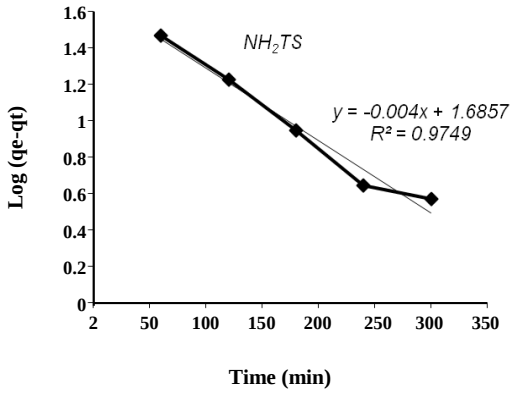

Fig. 9: The pseudo-first-order kinetic plot of Th(IV) adsorption on TS and NH_2TS nanocomposites.

intervals. Fig. 8 shows the amount of Th(IV) adsorbed onto the nanocomposites as a function of time. To investigate the specific rate constant of the present adsorption reactions, the experimental data were analyzed using two kinetic model equations including pseudo-first-order and pseudo-second-order ones [37, 38]. The pseudo-first-order model equation is written in Eq. (5):

$$\log(q_e - q_t) = \log q_e - \frac{k_1}{2.303} t \qquad (5)$$

Where qe and qt are the amounts of metals adsorbed on the sorbent (mg/g) in equilibrium and at time t, respectively, and k_1 is the rate constant of the first-order adsorption (min^{-1}). The straight line plots of log (qe-qt) against t were used to determine the rate constant (k_1) and correlation coefficient (R^2) values of the model (Fig. 9). The calculated pseudo-first-order correlation coefficients for TS and NH_2TS sorbents and the values of constants are given in Table 2.

Effect of the contact time on removal of thorium ion and adsorption kinetics

Fig. 8 shows the effect of the contact time on the Kd values of Th(IV) for the TS and NH_2TS adsorbents. The distribution coefficient (Kd) of Th(IV) on the prepared composite adsorbents was measured as a function of contact time, from 1 to 22 h time intervals. At the end of each time interval, the solution was filtered for phase separation and the concentration of supernatant solutions was measured. The adsorption of Th(IV) increased with increasing contact time and reached a maximum value after 5 h on both TS and NH_2TS. Hence, a contact time of 5 h was chosen for further studies.

The rate of adsorption of Th(IV) was initially fast and then reached a plateau value. The high adsorption rate

Table 2: Kinetic Parameters for Th(IV) sorption onto the NH_2TS and TS nanocomposites.

		Pseudo-first-order model			Pseudo-second-order model		
Adsorbent	$q_{e\,(exp)}$ (mg/g)	$K_1(min^{-1})$	q_e (mg/g)	R^2	K_2 (g/mg min)	q_e (mg/g)	R^2
TS	13.8	6.909×10^{-3}	14.2	0.9754	$8.95.3\times10^{-4}$	14.2	0.9924
NH_2TS	52.1	9.212×10^{-3}	48.5	0.9749	3.170×10^{-4}	54.9	0.9981

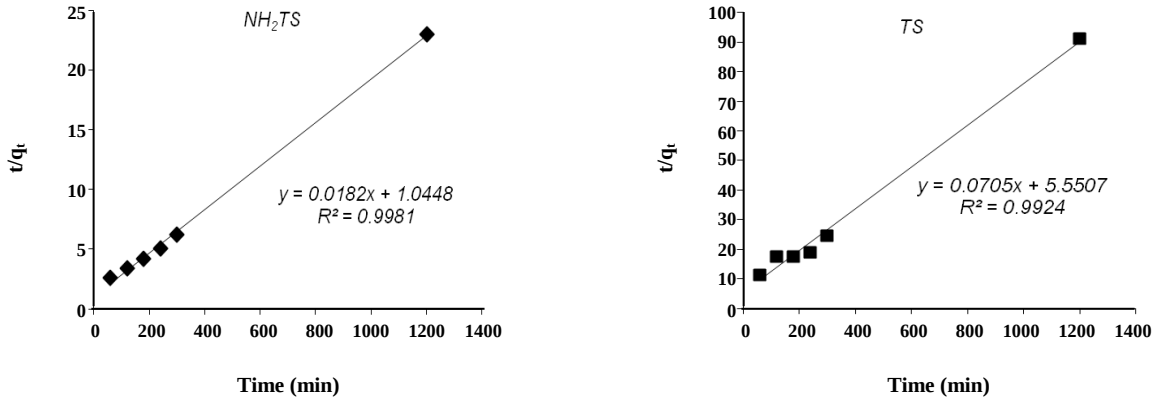

Fig. 10: The pseudo-second-order kinetic plot of Th(IV) adsorption on NH_2TS and TS nanocomposites.

was due to the abundance of active binding sites on the adsorbents, and as these sites were saturated, only a reduced amount of adsorption was occurred. This finding is in consistence with *Costa et al.* reports [36].

The mathematical expression of the pseudo-second-order model is shown in Eq. (6):

$$\frac{t}{q_t}=\frac{1}{k_2 q_e^2}+\frac{t}{q_e} \qquad (6)$$

Where t is time (min), qt and qe are the quantity of the adsorbed ions on the surface of the sorbent (mg/g) at time t and in equilibrium, respectively. k_2 denotes the pseudo-second-order rate constant (g/mg·min). The values of constants and correlation coefficients for pseudo-second-order can be calculated from the slope and intercept of the plot of t/qt versus t (Fig. 10). The calculated pseudo-second-order correlation coefficients for TS and NH_2TS sorbents and the values of constants are shown in Table 2.

The R^2 values obtained from the pseudo-first-order kinetic plots are relatively small and the experimental qe values are not consistent with the values calculated from the linear plots.

The correlation coefficients of pseudo-second order kinetics are higher than those of the pseudo-first order ones. Besides, the nearly comparable experimental qe and caculated qe values obtained from pseudo second- order equations imply that the the adsorption of Th(IV) on TS and NH_2TS is more fitted to the pseudo-second order kinetic.

The difference in the sorption efficiency of the Th(IV) metal ions onto TS and NH_2TS can be explained on the basis of more affinity of the surface of NH_2TS with the thorium metal ions. As far as we are concerned, the NH_2TS as an inorganic–organic hybrid material can act as a good chelating agent in pollutant Th(IV) ion removal from aqueous solution. Essentially, NH_2TS shows good sorption performance for Th(IV) in comparison with many adsorbents reported in literature. In order to evaluate the maximum adsorption capacity (q_{max}) of Th(IV) adsorption on the surface of NH_2TS, some adsorption experiments with varying Th(IV) concentration have been performed at the pH 5 and temperature 298.15 K. The corresponding experimental data, which is well fitted by the Langmuir isotherm (R = 0.946) are presented in Fig. 11. Langmuir equation which is used for monolayer adsorption on finite and similar surfaces has the form of Eq. (7) [39].

$$\frac{C_e}{q_e}=\frac{1}{q_{max} b}+\frac{C_e}{q_{max}} \qquad (7)$$

Table 3: Comparison of maximum adsorption capacity (q_{max}) of synthesized NH_2TS nanocomposite towards Th(IV) with various adsorbents for thorium ions

Adsorbent	q_{max} (mg /g)	pH	Temperature (K)	Ref.
Tin oxide	62.5	6	298.15	[1]
Silica–SH	412.54	4	298.15	[40]
Silica–NH2	431.19	4	298.15	[40]
Sodium clinoptilolite	333.3	4	313.15	[41]
PEO/PLLA (poly ethylene oxide/ polyL-lactide)	50.1	6	298.15	[42]
bi-functionalized biocomposite	26.92	4	298.15	[43]
chitosan entrapped in polyacrylamide hydrogel	118.34	5	298.15	[44]
Titanium phosphate	81.2	3	333.15	[45]
Al-pillared rectorite	30.16	1.88	293.15	[46]
oxidized multi-wall carbon nanotubes	13.22	1.9	293.15	[47]
nanocrystalline MOR type zeolite	360	5	303.15	[26]
nanoporous ZnO	1500	5	303.15	[48]
NH_2TS	1000	5	298.15	This study

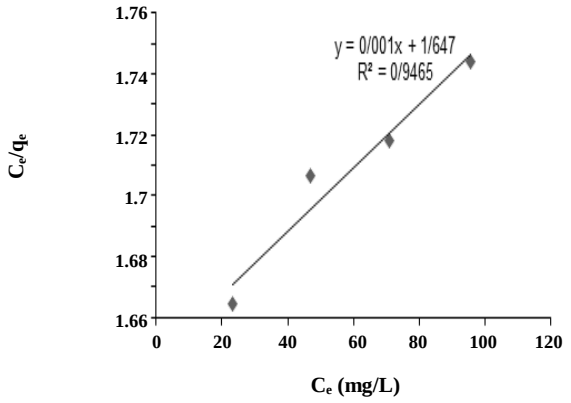

Fig. 11: Langmuir isotherm for adsorption of Th(IV) by NH_2TS.

where q_{max} is the maximum monolayer adsorption capacity (mg/g), KL is the Langmuir constant related to the free energy of adsorption (L/mg), and a plot of Ce/qe versus Ce yields a straight line with slope 1/qm.

The obtained q_{max} value is compared to the values reported in the literature for different adsorbent materials in Table 3. A highe adsorption capacity for NH_2TS compared to most of presented adsorbents in the Table 3 is seen.

CONCLUSIONS

Mesoporous TiO_2-SiO_2 (TS) and amino-functionalized TiO_2-SiO_2 (NH_2TS) nanocomposites were successfully synthesized and used as sorbents for thorium ion removal. The specific surface area decreased by 49% after the grafting of APTES on TS mater. In detail, the pore size of NH_2TS (3.63 nm) was smaller than that of TS (4.65 nm) due to the organic chain, but the particle size of NH_2TS was larger.

In spite of the poorer prosity properties of NH_2TS, it exhibited exceptional ability of sorption into the Th(IV) ion compared to TS. In conclusion, the study of the thorium ion adsorption onto the TS and NH_2TS nanocomposites demonstrated that the NH_2TS inorganic–organic hybrid material could act as a promising chelating agent in pollutant Th(IV) ion removal from aqueous solution. The batch studies for TS and NH_2TS were followed to give a good number of favourable thermodynamic and kinetic sets of data such as endothermic enthalpy, negative free Gibbs energy, positive entropic values, and pseudo second- order sorption model. These thermodynamic and kinetic data suggest the application of the amino-functionalized TiO_2-SiO_2 (NH_2TS) material for more effective sorption of thorium ion from aqueous solution. Also, according to Langmuir isotherm, maximum adsorption capacity (qm) is 1000 mg/g for NH_2TS which is a high value in comarision with value reported for other adsornents and implies a high capability of NH_2TS for the adsorption of Th(IV) ion from an aqueous solution.

Received : Jun 2, 2018 ; Accepted : Dec. 3, 2018

REFERENCES

[1] Nilchi A., Shariati Dehaghan T., Rasouli Garmarodi S., Kinetics, Isotherm and Thermodynamics for Uranium and Thorium Ions Adsorption from Aqueous Solutions by Crystalline Tin Oxide Nanoparticles, *Desalination*, **321**: 67–71 (2013).

[2] Thorium Dioxide

[3] Youngju J., Seok K., Soo-Jin P., Ji Man K., Application of Polymer-modified Nanoporous Silica to Adsorbents of Uranyl Ions, *Colloi. Surf. A.*, **313–314**:162–166 (2008).

[4] Kadirvelu K.; Thamaraiselvi K.; Namasivayam C., Removal of Heavy Metals from Industrial Wastewaters by Adsorption onto Activated Carbon Prepared from an Agricultural Solid Waste, *Bioresour. Technol.*, **76**: 63-65 (2001).

[5] Shao D.D., Jiang Z.Q., Wang X.K., Li J.X., Meng Y.D., Plasma induced Grafting Carboxymethyl Cellulose on Multiwalled Carbon Nanotubes for the Removal of UO_2^{2+} from Aqueous Solution, *J. Phys. Chem. B.*, **113**: 860–864 (2009).

[6] Yang X., Li J.X., Wen T., Ren X.M., Huang Y.S., Wang X.K., Adsorption of Naphthalene and Its Derivatives on Magnetic Graphene Composites and the Mechanism Investigation, *Colloid. Surf. A.*, **422**:118–125 (2013).

[7] Li J.X., Guo Z.Q., Zhang S.W., Wang X.K., Enrich and Seal Radionuclides in Magnetic Agarose Microspheres, *Chem. Eng. J.*, **172**: 892–897 (2011).

[8] Chen H., Shao D., Li J., Wang X., The Uptake of Radionuclides from Aqueous Solution by poly(amidoxime) Modified Reduced Graphene Oxide, *Chem. Eng. J.*, **254**: 623–634 (2014).

[9] Huang S.H., Chen D. H., Rapid Removal of Heavy Metal Cations and Anions from Aqueous Solutions by an Amino-Functionalized Magnetic Nano-Adsorbent, *J. Hazard. Mater.*, **163**: 174-179 (2009).

[10] Mahdavian A.R., Mirrahimi M.A.S., Efficient Separation of Heavy Metal Cations by Anchoring Polyacrylic Acid on Superparamagnetic Magnetite Nanoparticles Through Surface Modification, *Chem. Eng. J.*, **159**: 264-271 (2010).

[11] Xu P., Zeng G.M., Huang D.L., Feng C.L., Hu S., Zhao M.H., Lai C., Wei Z., Huang C., Xie G.X., Liu Z.F., Use of Iron Oxide Nanomaterials in Wastewater Treatment., *Sci. Total. Environ.*, **424**: 1-10 (2012).

[12] Nilchi A., Rasouli Garmarodi S., Janitabar Darzi S., Adsorption Behavior of Nano Sized Sol-Gel Derived TiO_2-SiO_2 Binary Oxide in Removing Pb^{2+} Metal Ions, *Separ. Sci. Technol.*, **45**: 801–808 (2010).

[13] Nilchi A., Janitabar Darzi S., Mahjoub A.R., Rasouli Garmarodi S., New TiO_2/SiO_2 Nanocomposites-Phase Transformations and Photocatalytic Studies, *Colloid. Surf. A.*, **361**: 25–30 (2010).

[14] Peshev P., Stambolova I., Vassilev S., Stefanov P., Blaskov V., Starbova K., Starbov N., pyrolysis Deposition of Nanostructured Zirconia Thin Films, *Mater. Sci. Eng. B.*, **97**:106–110 (2003).

[15] Marcoux L., Florek J., Kleitz F., Critical assessment of the Base Catalysis Properties of Amino-Functionalized Mesoporous Polymer-SBA-15 Nanocomposites, *App. Catal. A. Gen.*, **504**:493-503 (2015).

[16] Guillet-Nicolas R., Marcoux L., Kleitz F., Insights into Pore Surface Modification of Mesoporous Polymer–Silica Composites: Introduction of Reactive Amines, *New. J. Chem.*, **34**:355–366 (2010).

[17] Zelenak V., Halamova D., Gaberova L., Bloch E., Llewellyn P., Amine-Modified SBA-12 Mesoporous Silica for Carbon Dioxide Capture: Effect of Amine Basicity on Sorption Properties, *Micropor. Mesopor. Mat.*, **116**:358–364 (2008).

[18] Song B.Y., Eom Y., Lee T.G., Removal and Recovery of Mercury from Aqueous Solution Using Magnetic Silica Nanocomposites, *Appl. Surf. Sci.*, **257**:4754–4759 (2011).

[19] Idris S.A., Harvey S.R., Gibson L.T., Selective Extraction of Mercury (II) from Water Samples Using Mercapto Functionalised-MCM-41 and Regeneration of the Sorbent Using Microwave Digestion, *J. Hazard. Mater.*, **193**: 171-176 (2011).

[20] Mureseanu M., Reiss A., Stefanescu I., David E., Parvulescu V., Renard G., Hulea V., Modified SBA-15 Mesoporous Silica for Heavy Metal Ions Remediation, *Chemosphere*, **73**:1499–1504 (2008).

[21] Manzano M., Aina V., Arean C.O., Balas F., Cauda V., Colilla M., Delgado M.R., Vallet-Reg M., Studies on MCM-41 Mesoporous silica for Drug Delivery: Effect of Particle Morphology and Amine Functionalization, *Chem. Eng. J.*, **137**:30–37 (2008).

[22] Liu H, Zhang L, Seaton N.A. Analysis of Sorption Hysteresis in Mesoporous Solids Using a Pore Network Model, *J. Colloid. Interf. Sci.*, **156**: 285-293 (1993).

[23] Kruk M., Jaroniec M., Sayari A., Application of Large Pore MCM-41 Molecular Sieves To Improve Pore Size Analysis Using Nitrogen Adsorption Measurements, *Langmuir*., **13**:6267-6273 (1997).

[24] Kruk M., Jaroniec M., Gas Adsorption Characterization of Ordered Organic−Inorganic Nanocomposite Materials, *Chem Mater*., **13**:3169–3183 (2001).

[25] Li W.J., Tao Z.Y., Comparative Study on Th(IV) Sorption on Alumina and Silica from Aqueous Solutions, *J. Radioanal. Nucl. Chem*., **254**:187–192 (2002).

[26] Sharma P., Tomar R., Sorption Behaviour of Nanocrystalline MOR Type Zeolite for Th(IV) and Eu(III) Removal from Aqueous Waste by Batch Treatment, *J. Colloid. Interf. Sci.*, **362**:144–156 (2011).

[27] Anirudhan T.S., Sreekumari S.S., Adsorptive Removal of Heavy Metal Ions from Industrial Effluents Using Activated Carbon Derived from Waste Coconut Buttons, *J. Environ. Sci.*, **23**: 1989–1998 (2011).

[28] Baes C.F., Mesmer R.E., "Hydrolysis of Cations", Jahn Wiley & Sons Inc., New-York (1976).

[29] Martins R.J.E., Pardo R., Boaventura R.A.R., Cadmium(II) and Zinc(II) Adsorption by the Aquatic Moss Fontinalis Antipyretica: Effect of Temperature, pH and Water Hardness, *Water. Res.*, **38**:693-699 (2004).

[30] Echeverria J.C., Zarranz I., Estella J., Garrido J.J., Simultaneous Effect of pH, Temperature, Ionic Strength, and Initial Concentration on the Retention of Lead on Illite, *Appl. Clay. Sci.*, **30**: 103-115 (2005).

[31] Sharma P., Tomar R., Synthesis and Application of an Analogue of Mesolite for the Removal of Uranium(VI), Thorium(IV), and Europium(III) From Aqueous Waste, *Micropor. Mesopor. Mater.*, **116**: 641-652 (2008).

[32] Anirudhan T.S., Jalajamony S., Ethyl Thiosemicarbazide Intercalated Organophilic Calcined Hydrotalcite as a Potential Sorbent for the Removal of Uranium (VI) and Thorium (IV) Ions from Aqueous Solutions, *J. Environ. Sci.*, **25**: 717–725 (2013).

[33] Cortes-Martínez R., Olguin M.T., Solache-Rios M., Cesium Sorption by Clinoptilolite-Rich Tuffs in Batch and Fixed-Bed Systems, *Desalination*., **258**: 164–170 (2010).

[34] Nilchi A., Rasouli Garmarodi S., Janitabar Darzi S., Removal of Arsenic from Aqueous Solutions by an Adsorption Process with Titania–Silica Binary Oxide Nanoparticle Loaded Polyacrylonitrile Polymer, *J. Appl. Polym. Sci.*, **119**: 3495–3503 (2011).

[35] Wu L., Ye Y., Liu F., Tan C., Liu H., Wang S., Wang J., Yi W., Wu W., Organo-Bentonite-Fe_3O_4 Poly (Sodium Acrylate) Magnetic Superabsorbent Nanocomposite: Synthesis, Characterization, and Thorium(IV) Adsorption, *Appl. Clay. Sci.*, **83–84**: 405–414 (2013).

[36] Da Costa A.C.A., Leite S.G.F., Metals Biosorption by Sodium Alginate Immobilized Chlorella Homosphaera Cells, *Biotechnol. Lett.*, **13**: 559–562 (1991).

[37] Abbasizadeh S., Keshtkar A.R., Mousavian M.A., Preparation of a Novel Electrospun Polyvinyl Alcohol/Titanium Oxide Nanofiber Adsorbent Modified with Mercapto Groups for Uranium(VI) and Thorium(IV) Removal from Aqueous Solution, *Chem. Eng. J.*, **220**:161–171 (2013).

[38] Ahmadi S.J., Akbari N., Shiri-Yekta Z., Mashhadizadeh M.H., Hosseinpour M., Removal of Strontium Ions from Nuclear Waste Using Synthesized Mno_2-Zro_2 Nano-Composite by Hydrothermal Method in Supercritical Condition, *Korean. J. Chem. Eng.*, **32**: 478-485 (2014).

[39] Wu Y., Kim S.Y., Tozawa D., Ito T., Tada T., Hitomi K., Kuraoka E., Yamazaki H., Ishii K., Equilibrium and Kinetic Studies of Selective Adsorption and Separation for Strontium Using Dtbu- CH18C6 Loaded Resin, *J. Nucl.Sci. Technol.*, **49**:320-327 (2012).

[40] Humelnicu D., Blegescu C., Ganju D., Removal of Uranium(VI) and Thorium(IV) Ions from Aqueous Solutions by Functionalized Silica: Kinetic and Thermodynamic Studies, *J. Radioanal. Nucl. Chem.*, **299**:1183–1190 (2014).

[41] Khazaei Y., Faghihian H., Kamali M., Removal of Thorium from Aqueous Solutions by Sodium Clinoptilolite, *J. Radioanal. Nucl. Chem.*, **289**:529-536 (2011).

[42] Savva I., Efstathiou M., Krasia-Christoforou T., Pashalidis I., Adsorptive Removal of U(VI) and Th(IV) from Aqueous Solutions Using Polymer-Based Electrospun PEO/PLLA Fibrous Membranes. *J. Radioanal. Nucl. Chem.*, **298**:1991-1997 (2013).

[43] Gok C., Turkozu D.A., Aytas S., Removal of Th(IV) Ions from Aqueous Solution Using Bi-Functionalized Algae-Yeast Biosorbent, *J. Radioanal. Nucl. Chem.*, **287(2)**: 533–541 (2011).

[44] Akkaya R., Ulusoy U., Adsorptive Features of Chitosan Entrapped in Polyacrylamide Hydrogel for Pb2+, UO22+, and Th4+., *J. Hazard. Mater.*, **151**(2–3): 380–388 (2008).

[45] Maheri K., Chudasam U., Studies on Kinetics, Thermodynamics and Sorption Characteristics of an Inorganic Ion Exchanger—Titanium Phosphate Towards Pb(II), Bi(III) And Th(IV), *J. Indian. Inst. Sci.*, **86**(5): 515-525 (2006).

[46] Yu S.M., Chen C.L., Chang P.P., Wang T.T., Lu S.S., Wang X.K., Adsorption of Th(IV) Onto Al-Pillared Rectorite: Effect of Ph, Ionic Strength, Temperature, Soil Humic Acid and Fulvic Acid, *Appl. Clay Sci.*, **38**(3–4): 219-226 (2008).

[47] Chen C.L., Li X.L., Zhao D.L., Tan X.L., Wang X.K., Adsorption Kinetic, Thermodynamic and Desorption Studies of Th(IV) On Oxidized Multi-Wall Carbon Nanotubes, *Colloid. Surf. A-Physicochem. Eng. Aspects*, **302** (1-3): 449–454 (2007).